

# FUNDAMENTAL STUDIES OF CRYSTAL GROWTH OF MICROPOROUS MATERIALS

Ramsharan Singh,<sup>1</sup> John Doolittle Jr.,<sup>1</sup> Pramatha Payra,<sup>1</sup> Prabir K. Dutta,<sup>1,\*</sup>  
Michael A. George,<sup>2</sup> Narayanan Ramachandran,<sup>3</sup> and Brian J. Schoeman<sup>4</sup>

<sup>1</sup>Department of Chemistry, The Ohio State University, Columbus, Ohio, <sup>2</sup>Department of Chemistry, University of Alabama, Huntsville, Alabama, <sup>3</sup>USRA, MFSC, Huntsville, Alabama, <sup>4</sup>Dow Chemical, Midland, Michigan

## Introduction

Microporous materials are framework structures with well-defined porosity, often of molecular dimensions. Zeolites contain aluminum and silicon atoms in their framework and are the most extensively studied amongst all microporous materials. Framework structures with P, Ga, Fe, Co, Zn, B, Ti and a host of other elements have also been made. Typical synthesis of microporous materials involve mixing the framework elements (or compounds, thereof) in a basic solution, followed by aging in some cases and then heating at elevated temperatures. This process is termed hydrothermal synthesis, and involves complex chemical and physical changes. Because of a limited understanding of this process, most synthesis advancements happen by a trial and error approach. There is considerable interest in understanding the synthesis process at a molecular level with the expectation that eventually new framework structures will be built by design. The basic issues in the microporous materials crystallization process include:

- Nature of the molecular units responsible for the crystal nuclei formation
- Nature of the nuclei and nucleation process
- Growth process of the nuclei into crystal
- Morphological control and size of the resulting crystal
- Surface structure of the resulting crystals
- Transformation of frameworks into other frameworks or condensed structures

The NASA-funded research described in this report focuses to varying degrees on all of the above issues and has been described in several publications.<sup>1-9</sup> Following is the presentation of the highlights of our current research program. The report is divided into five sections:

1. Fundamental aspects of the crystal growth process
2. Morphological and surface properties of crystals
3. Crystal dissolution and transformations
4. Modeling of crystal growth
5. Relevant microgravity experiments

## 1. Fundamental aspects of the crystal growth process

### *1.1 Reverse micellar system and microporous zincophosphate synthesis*

We have focused on a novel synthesis medium to provide basic information about microporous crystal growth. Reverse micelles are thermodynamically stable systems, where ionic and nonionic surfactant

**Keywords:** zeolite, reverse micelle, modeling, nanoparticles, AFM

\*Corresponding author, e-mail: [dutta@chemistry.ohio-state.edu](mailto:dutta@chemistry.ohio-state.edu)

molecules in hydrocarbon solvents solubilize water in small nanoclusters. The water pool of the reverse micelles have been used extensively for synthesis of a wide range of size-quantized dispersed inorganic nanoparticles.<sup>10</sup> We were the first to report that microporous materials can also be synthesized under the appropriate conditions in reverse micellar reactants.<sup>7,8</sup> Figure 1 compares the frameworks of sodalite, faujasite, zeolite A and hopeite which are relevant to the present study.

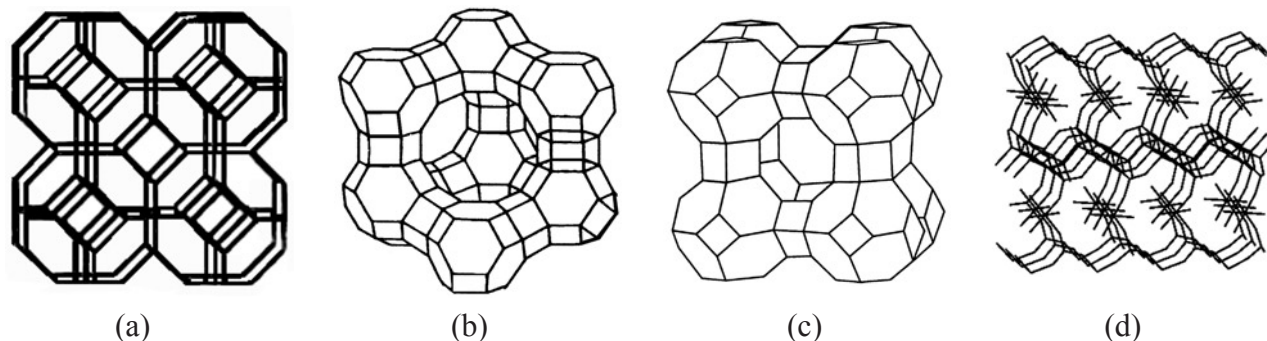


Figure 1. Framework structures of (a) Sodalite, (b) Faujasite, (c) Zeolite-A and (d) Hopeite.

The reverse micelle based synthesis of microporous materials involves mixing together reactants contained in reverse micelle solutions. The important steps in formation of crystal nuclei involve exchange processes between reverse micelles, as depicted in Figure 2. Because the reactants remain encapsulated in reverse micelles throughout the synthesis process, the chemistry within the nanometer sized water pools determine the crystal growth dynamics.



Figure 2. Exchange processes in reverse micelles.

**1.1.a Sodalite system.** The most extensively used surfactant for reverse micelle synthesis is sodium bis(2-ethylhexyl) sulfosuccinate (AOT). We have reported the synthesis of zincophosphate sodalite (ZnPO-S) microporous material using AOT reverse micelles.<sup>7,8</sup> If reactant composition is chosen such that only a small fraction of the micelles have the right supersaturation to form nuclei, then these nuclei can commence crystal growth using up the non-nucleated reverse micelles. After the crystals reach a certain size, they begin to settle via gravity, avoiding further growth in size. On the other hand, if the reactant composition is such that supersaturation is exceeded in a large fraction of the micelles, then rapid precipitation of an amorphous solid can occur, resembling the conventional synthesis. This control over crystallization pathways by minor changes in the reactant composition is unique to the reverse micellar medium and is a reflection of chemistry within the water pools.

However, AOT-based reverse micelles could not be used for synthesis of open frameworks. The aqueous environment within the AOT reverse micelles was not appropriate for microporous material synthesis.<sup>6</sup> Use of cationic reverse micelles, especially the two-tailed surfactant dimethyldioctylammonium chloride (DODMAC) resulted in the successful synthesis of faujasitic ZnPO-X.<sup>4,5</sup>

**1.1.b Faujasitic System (ZnPO-X).** The primary goal of using DODMAC reverse micelles was to synthesize porous zincophosphate frameworks, in particular ZnPO-X. Two templating agents have

been studied, tetramethylammonium ion ( $\text{TMA}^+$ ) and 1,4-diazabicyclo[2,2,2]octane (DABCO). Mixing proper ratio of Zn, phosphate and TMAOH containing reverse micelle solutions (made by the equilibration method) produced ZnPO-X crystals. Upon ultracentrifugation of the mother liquor before any cloudiness was visually evident, a small amount of solid was recovered. These suspended crystals are small, on the order of a few hundred nm. Enough sample could not be recovered for diffraction analysis, but micro Raman spectroscopy showed bands at 765, 983, 1014 and 1119  $\text{cm}^{-1}$ , characteristic of faujasitic zincophosphate (ZnPO-X).<sup>6</sup>

With DABCO as templating agent, the DODMAC reverse micelles were made by an injection method. Light scattering experiments showed that the diameter of the **Zn** and **P** containing reverse micelles were 8 nm and 6 nm respectively. Reaction was carried out by mixing the **Zn** and **P** micelles with volume ratio of 1:1. Powder diffraction patterns as well as the octahedral morphology confirm the formation of the ZnPO-X structure. The yields of zincophosphate X were of the order of 15-20%, indicating that a large fraction of the zinc and phosphate species were still present in the micellar medium, with the size of the clusters remaining in solution being of the order of 15 nm.<sup>4</sup>

## **1.2 Nucleation and Control of Crystal Growth**

**1.2.a Reverse Micelle System.** Reverse micellar systems also provided a novel medium for studying “seeding” phenomena in growth of microporous materials. The addition of seed crystals to speed up the crystallization process has been practiced for microporous material synthesis for four decades.<sup>11</sup> The mechanism for rate enhancement is eventually related to the small size seeds. Macroscopic seeds promote nucleation by providing nuclei that exists on their surfaces (secondary process) and small seeds by virtue of their high surface area consume reactants and grow rapidly into crystals.

We examined the hypothesis that the 15 nm particles left behind from a ZnPO-X synthesis had a memory of the crystal and should act as an effective seed solution. To use the mother liquor as an effective seed solution, a second micellar composition (**B**) was prepared. This composition does not produce ZnPO-X. Upon adding the mother liquor to composition **B**, uniform ZnPO-X crystals were produced. The seeding experiments were repeated in columns of heights 0.71, 1.78 and 2.62 meters, and the crystal sizes increased with average sizes of 3, 6 and 15  $\mu\text{m}$  crystals of ZnPO-X.<sup>4</sup>

**1.2.b Aluminosilicate System.** Since the nanometer-sized entities left behind were found to be effective in growing crystals in reverse micelle system (Section 1.2.a), we have extended this concept to aluminosilicate zeolites. In this system we synthesize nanometer-sized zeolite particles in clear solution synthesis following procedures developed by Schoeman and coworkers.<sup>12,13</sup> The yield of nanometer-sized zeolite particles synthesized in clear solution system is very low. This is in parallel to our observation for ZnPO-X reverse micelle synthesis. We propose that this is because certain nutrients are exhausted from the synthesis system, thus stopping the further growth of the nuclei or nano-particles already in the system. Our hypothesis is that the species remaining behind in solution has ‘memory’ of the system and if provided with nutrients, will grow into crystals.

To establish our hypothesis in aluminosilicate clear solution system, we chose zeolites Y, A and sodalite system. The framework structures of these zeolite systems are shown in Figure 1. The nanometer-sized particles of zeolite-Y, A and Sodalite were synthesized using previously published procedures.<sup>12,13</sup> After removing the crystallized nano particles of zeolite material, the remaining clear solution was used

as ‘nuclei’ for seeding experiments. A composition of  $15.2\text{TMA}_2\text{O}:x\text{Na}_2\text{O}:1.6\text{Al}_2\text{O}_3:45\text{SiO}_2:805\text{H}_2\text{O}$  was chosen as a source of nutrient solution for these experiments. The amount of sodium content was controlled by adjusting the pH of silica sol reactant to 8 by means of ion exchange using a cation-exchange resin, Dowex HCR-S( $\text{H}^+$ ). This reaction mixture produces small amounts of sodalite after 3 days. We have found that zeolites Y, A and Sodalite can be synthesized by using their respective ‘nuclei’ solution as seed (nutrient to seed volume ratio 8). Thus, synthesis of these zeolites namely Y, A and Sodalite from identical nutrient solutions demonstrates the memory effect of ‘nuclei’ seeds as the controlling feature in the crystallization. Previous studies have focused on macroscopic seeds. Our contribution has been to show that ‘memory’ of crystals is retained even in nanometer-sized particles that do not have characteristics of a well-formed crystal.

## 2. Morphological and Surface Properties of Crystals

### 2.1 Morphological Control

Morphological control of microporous crystalline materials via synthetic routes is important for several reasons. For instance, it provides information about parameters that control nucleation and crystal growth, thereby illuminating aspects of the synthesis mechanism. Also, control of morphology is important for targeting various applications. We have shown that by altering composition, the morphology ZnPO-X could be changed.<sup>9</sup> Previously reported synthesis of ZnPO-X at  $4^\circ\text{C}$  led to the formation of crystals with the characteristic octahedral morphology of faujasitic structures. Sizes of these crystals are in the  $<10\ \mu\text{m}$  range. We found that by increasing the TMAOH/ $\text{H}_3\text{PO}_4$  and  $\text{Zn}^{2+}/\text{Na}^+$  ratios, the morphology was drastically altered to produce large hexagonal platelet type crystals with diameters around  $100\ \mu\text{m}$ . Figure 3 demonstrates the morphological change. Based on electron microscopy data, we concluded that the presence of twin planes was leading to crystals with the platelet-like morphology.

### 2.2 Surface Structure

We have observed significant differences between surfaces of the microporous crystals synthesized via conventional hydrothermal method and reverse micelle method. Such differences have implications in both the growth mechanism and the usefulness of the crystals for various applications. From the SEM images of ZnPO-X synthesized by hydrothermal (HS) and reverse micelle (RM) methods, surface smoothness was evident on the crystals made by the RM method. This is more evident in the AFM images of the crystals shown in Figure 4.

Previous studies have concluded, in general that zeolitic open frameworks both grow and dissolve by a layer-by-layer mechanism.<sup>14</sup> Thus, at any time during crystal growth, a growing crystal face is bombarded by nuclei that can attach to the crystal face and start growing. Because of the random nature of the collisions, there are multiple nucleation sites on the crystal surface at which growth occurs. Eventually the growing faces meet and complete a layer on a surface, though during this time, crystal growth could have begun on top of the layer. Such a growth pattern will lead to multiple layers and we could readily distinguish  $\sim 20$ -25 layers on the ZnPO-X crystal surface (Figure 4a). For aluminosilicate faujasites, a structure with similar framework as ZnPO-X, Anderson and coworkers<sup>14</sup> noted triangular terraces with step heights of approximately  $15\text{\AA}$ , which is the dimension of a faujasite sheet, and the present studies are consistent with these observations. Thus, it appears that the ZnPO-X HS sample has features very similar to those reported for aluminosilicate zeolites, and suggest similar growth mechanisms.

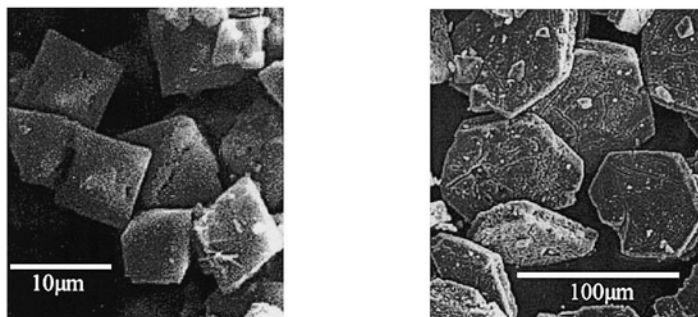


Figure 3. SEM micrographs of ZnPO-X crystals demonstrating the change in morphology from octahedral crystals (left) to platelet crystals (right).

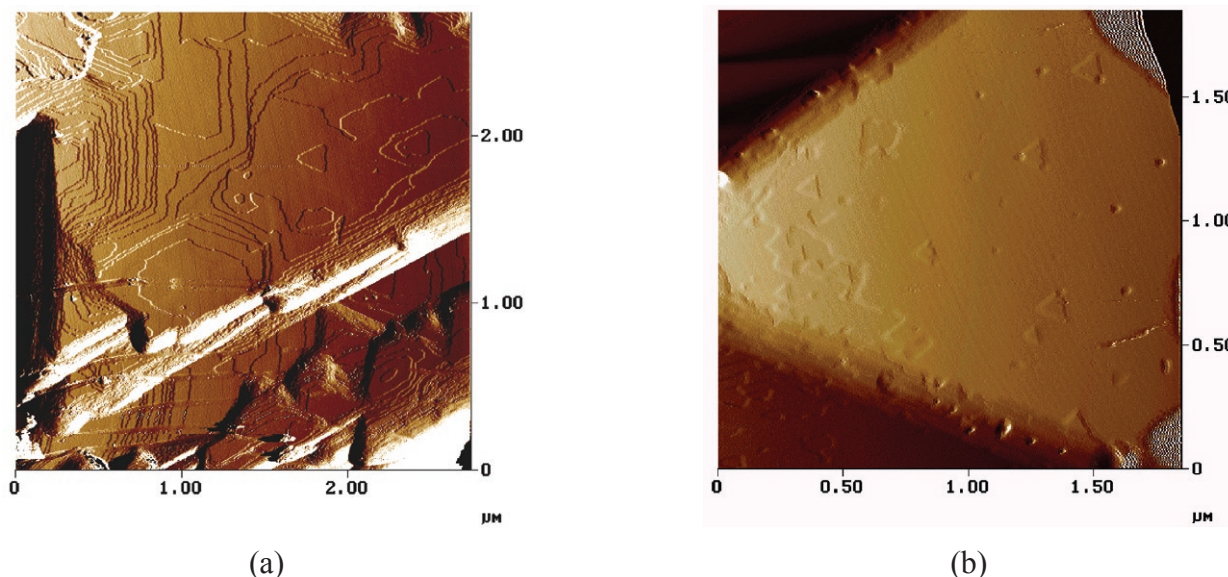


Figure 4. AFM images of the ZnPO-X surface synthesized via (a) hydrothermal synthesis method and (b) reverse micelle system.

On the other hand, crystals grown by the RM method show distinct differences from the HS grown crystals. Besides the differences in the surface roughness due to the lack of terraces on the (111) face, there is another important difference as is clear from Figure 4. The few triangular terraces noticed on the RM crystals have their orientations in registry with the overall crystals, with the apex of the triangle pointing to the crystal edges and not rotated, as was noted earlier for the HS grown crystals.

Nucleation in the RM system begins in tiny water droplets that are dispersed in an organic medium. Crystal growth proceeds by acquiring nutrients from the aqueous interior of the reverse micelles that collide with the crystal surface. Since the zincophosphate crystal is growing in an organic medium and the crystal surface is polar, it is likely that the growing crystal is covered by a film of water separated from the hydrocarbon by a layer of surfactant molecules. Such an arrangement will stabilize the polar crystal surface-hydrocarbon interface. Thus, when reverse micelles containing the nutrients collide with the crystal surface, its contents get distributed in the water layer surrounding the crystal. This water layer provides a means for the nutrients to re-equilibrate and provide building blocks for the growth of the crystal. The absence of terraces in the RM samples indicates that terrace nucleation is slower as compared to propagation of the layer across the surface.

The growth in the RM system is fundamentally different because of the presence of the protective surface water layer, which equilibrates and minimizes the number of species involved in crystal growth.

### 3. Crystal Dissolution and transformations

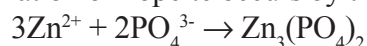
#### 3.1 Dissolution of ZnPO-X

The possibility of synthesizing reasonably large flat crystals of ZnPO-X has made it feasible to do detailed Raman microprobe spectroscopic experiments. In particular, we have focused on microprobe Raman spectroscopy and examined how dissolution of ZnPO-X crystals occurs as a function of different monovalent cations in the medium.<sup>2</sup> The vibrational information obtained from Raman spectroscopy made it possible to analyze the structural changes at the molecular level. In the presence of H<sup>+</sup>, at a pH of 3, the vibrational bands due to ZnPO-X disappeared completely in 12 minutes. These were replaced by Raman bands of hopeite, Zn<sub>3</sub>(PO<sub>4</sub>)<sub>2</sub>, a condensed form of zincophosphate. Electron microscopic experiments showed that the ZnPO-X was gradually getting covered with a film of hopeite. If, instead of H<sup>+</sup>, Li<sup>+</sup>, or Cs<sup>+</sup> were used, then the ZnPO-X gradually converted to framework structures of LiA(BW) and CsZnPO<sub>4</sub>, respectively. How H<sup>+</sup>, Li<sup>+</sup> and Cs<sup>+</sup> destabilize in the ZnPO-X structure was also manifested in the vibrational band of tetramethylammonium (TMA) ions trapped in the sodalite cages of ZnPO-X. Upon exchange with H<sup>+</sup>, Li<sup>+</sup>, and Cs<sup>+</sup>, prior to collapse of the ZnPO-X and loss of TMA from the Raman spectra, there is a significant broadening of the TMA band at 765 cm<sup>-1</sup>. The bandwidth changes from ~ 6 cm<sup>-1</sup> for Na<sup>+</sup> to 11,12 and 16 cm<sup>-1</sup> for H<sup>+</sup>, Cs<sup>+</sup> and Li<sup>+</sup>, respectively. Our interpretation is that, upon ion-exchange with these cations, there is a distortion of the ZnPO-X framework, which makes the framework more susceptible to hydrolysis.

#### 3.2 Influence of Framework Topology on Dissolution

Dissolution of ZnPO-X and sodalite crystals were carried out using a citrate buffer of pH 3, and methodology for measuring the differences in the dissolution dynamics were developed.<sup>1</sup> The powder diffraction data clearly indicates that in both ZnPO-X and ZnPO-S dissolution, hopeite [Zn<sub>2</sub>(PO<sub>4</sub>)<sub>3</sub>] is being formed as the product at pH~3. Electron microscopy (Figure 5) shows that the morphology of the hopeite formed in both cases is quite distinct. In the ZnPO-X, the hopeite crystals are considerably smaller and form a dense coating on the surface of the ZnPO-X pellet. For ZnPO-S, the hopeite crystals are considerably larger, and do not completely cover the pellet surface.

Elemental analysis of the solution shows the presence of both zinc and phosphorus indicating the presence of M<sup>+</sup>(aq), Zn<sup>2+</sup>(aq) and PO<sub>4</sub><sup>3-</sup>(aq). Formation of hopeite occurs by the following reaction:



As the zincophosphate dissolves, supersaturation that initiates the nucleation of hopeite occurs around the pellet surface. The formation of hopeite is promoted because of its low solubility, K<sub>sp</sub> being reported on the order of 10<sup>-35</sup>.

A colorimetric method that monitors the pH change around the dissolving crystals provides a direct estimate of hopeite formation. Figure 6a shows a typical spectral change during dissolution. We have examined the dissolution of hopeite and find no change in pH around the dissolving crystal. The dissolution of the framework zincophosphate structures with Zn/P = 1:1, to form hopeite leads to the imbalance of Zn and phosphate that leads to the pH change. The increase in pH around the dissolving crystal can be readily explained as arising from reaction of PO<sub>4</sub><sup>3-</sup> with H<sup>+</sup> to form HPO<sub>4</sub><sup>2-</sup>/H<sub>2</sub>PO<sub>4</sub><sup>-</sup>. Thus, any changes in pH that we observe during ZnPO dissolution can be related to the excess phosphate resulting from formation of hopeite. The larger change in pH for the ZnPO-X system (Figure 6b) is consistent with the elemental

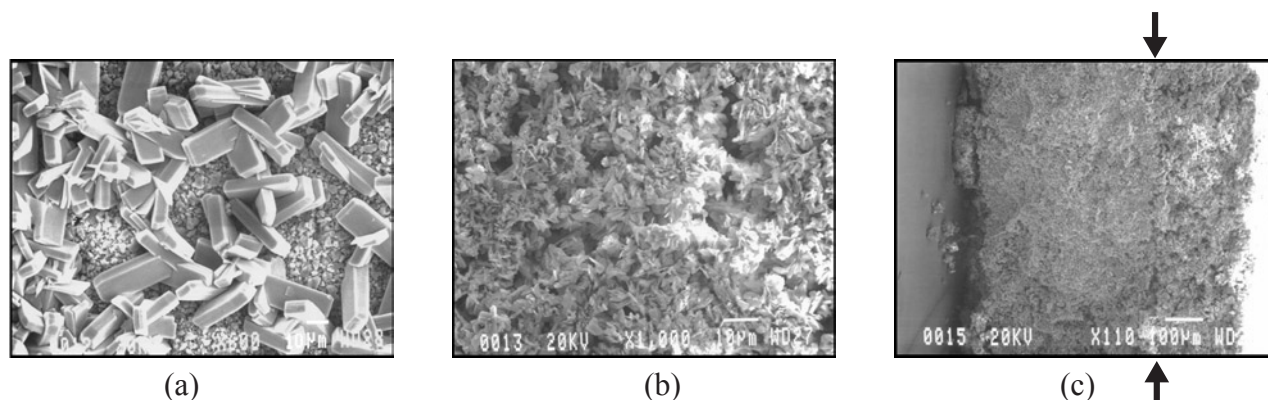


Figure 5. SEM micrographs of pellets of (a) ZnPO-S and (b) ZnPO-X after 1 hour of exposure to pH  $\sim$ 3 buffer (c) a side view of ZnPO-X after 2 hours of exposure to pH  $\sim$ 3 buffer (unstirred system). The layer to the right of the arrows is hopeite.

analysis data and supports the model that hopeite growth is more pronounced on ZnPO-X as compared to the ZnPO-S system.

### 3.3 Dissolution Mechanism.

The simplest possibility for hopeite formation is that the frameworks are dissolving to form Zn and phosphate, which then exceed supersaturation to form hopeite. However, considering the differences in morphology and the dynamics of hopeite formation and that the overall levels of solubilized zinc and phosphate are comparable, as seen from the elemental analysis, we do not favor this mechanism.

A more likely possibility is that the hopeite is nucleated on the surface of the dissolving crystal from the dissolution products prior to the species escaping into the solution. We propose the hypothesis that the nuclei of hopeite arise from intermediate dissolution products of the zincophosphate frameworks. Because of the differences in the framework structure and the access of protons to the framework, the dissolution units are structurally different, and result in formation of hopeite of distinct morphologies. Small crystals are expected to grow faster than larger crystals for diffusion-controlled processes. The pH studies indicate that the hopeite formation on ZnPO-X is more pronounced than ZnPO-S and could be a reflection of the smaller crystals and diffusion-controlled growth.

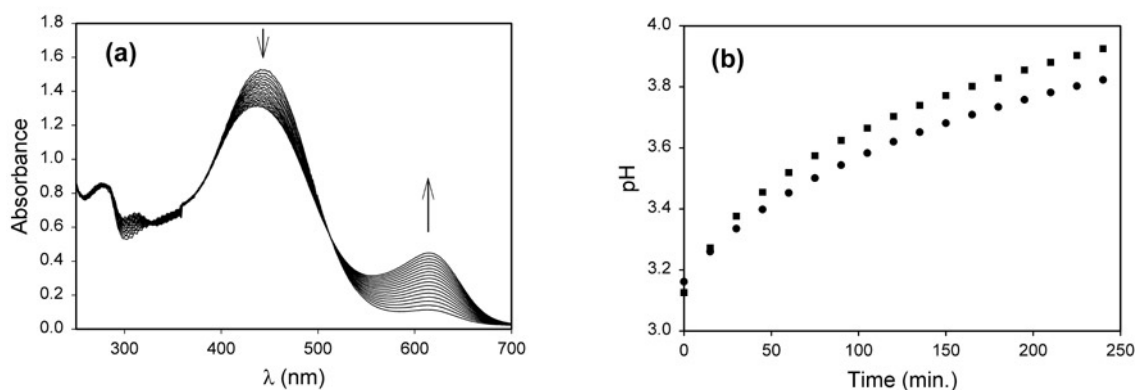


Figure 6. (a) Absorption spectra of the solution above a dissolving ZnPO-S pellet and (b) pH changes around dissolving ZnPO-S (●) and ZnPO-X (■) as a function of time (data taken every 15 min) in a solution containing bromocresol green buffered at pH  $\sim$ 3 (unstirred system).

#### 4. Modeling of Nucleation and Crystal Growth

Thompson and coworkers have pioneered the Population Balance model to model zeolite synthesis.<sup>15,16</sup> Recently there are reports of using population balance approach to study nucleation and crystal growth of nanoparticles such CdS and CaCO<sub>3</sub> in reverse micellar systems.<sup>17,18</sup> We are currently examining the feasibility of applying Population Balance modeling scheme to understand the nucleation and crystal growth of zincophosphate microporous materials from both reverse micelle based and hydrothermal synthesis.

##### 4.1 Theoretical Development

The analysis that follows will be strictly limited to batch systems, that are, closed systems for which there is no exchange of mass with the surroundings.

If the particle size distribution of the population at any time during the process is given by  $n = n(L, t)$ , then the population balance for the batch system described above is

$$\frac{\partial n}{\partial t} + Q \frac{\partial n}{\partial L} = 0 \quad (1)$$

where  $t$  is time,  $L$  is some characteristic particle size, and  $Q$  is the linear growth rate. An initial condition and a boundary condition are necessary to uniquely specify the solution of the population balance equation. These are, respectively,

$$n(L, 0) = n_0 \quad (2)$$

$$n(r, t) = 0 \quad (3)$$

where boundary condition at  $L = r$  accounts for the size of particles at time  $t$ . Rather than solve the partial differential equation, Equation (1), it is more convenient here to make use of the moment transformation to generate a set of ordinary differential equations that can be solved more easily. Thus, if in Equation (1) each term is multiplied by  $L^i$  and then integrated over all possible particle sizes, the resulting set of moment equations is

$$\frac{dm_0}{dt} = 0 \quad (4)$$

$$\frac{dm_1}{dt} = Qm_0 \quad (5)$$

$$\frac{dm_2}{dt} = 2Qm_1 \quad (6)$$

$$\frac{dm_3}{dt} = 3Qm_2 \quad (7)$$

where the moments of the particle size distribution, the  $m_i$ 's, represent the cumulative number, length, area, and volume of particles, respectively. These can be solved far more easily than Equation (1), as long as the growth rate,  $Q$ , is known.

The size-independent growth rate is given by

$$Q(C) = k_g (C - C_{critical}) \quad (8)$$

where  $C$  is the concentration of the intermediate species, and  $C_{critical}$  is the critical concentration of these species. It is assumed that the "activation reaction" sequence is solution occurs as



and that the transition from  $I$  (inactive) to  $C$  (active) occurs by some rate-limiting first-order reaction. As before, this assumption can be changed to reflect the specific nature of the chemical system of interest. The first-order reaction representation for the hydrolysis reaction has been used previously,<sup>19</sup> and provides a relatively simple way of assessing the effect of a chemical conversion prior to the onset of the precipitation. To complete the formulation of the problem, then, materials balances for the inactive and the active species are written as

$$\frac{dI}{dt} = -k_1 I \quad (10)$$

$$dC/dt = k_1 I - \rho \phi Q m_1 / 2. \quad (11)$$

where  $\rho$  is the solid molar density (moles/cm<sup>3</sup>) and  $\phi$  is the particle area shape factor (dimensionless). The last term in Equation (11) accounts for the consumption of active solution species by growth on existing particle surface.

Now to complete the formulation of the problem we must define the initial values. It is assumed that there is no nucleation and only the seed nuclei are growing, therefore, number of seed nuclei and hence the number of particles are constant throughout the reaction and it is known from the experimental data. Let the number of nuclei be  $n_0$ . With further assumption that the seed particles are spherical and uniform in size the initial value of moments are calculated to as follows:

$$m_0 = n_0 \quad (12)$$

$$m_1 = n_0 * (2r) \quad (13)$$

$$m_2 = n_0 * (4\pi r^2) \quad (14)$$

$$m_3 = n_0 * ((4/3) * \pi r^3) \quad (15)$$

where  $r$  is the radius of the initial ‘nuclei’ or ‘seed’ which can be determined experimentally. Now the initial values of all the moments are known because  $n_0$  and  $r$  are known. Initially  $C$  is zero and  $I = I_0$ . Now the problem is well defined. The Equations (4)-(15) (excluding Equation 9 of course) will yield information regarding the growth of the seed nuclei in presence of a solution of limited inactive nutrients after an activation reaction in the solution phase.

#### 4.2 Modeling of ZnPO-X seeded growth in reverse micelle system.

The equations noted above were solved using a standard fourth order Runge-Kutta integration procedure. For the preliminary results we are presenting here we made several assumptions to put the simulations in some perspective. We assume the reverse micelle nutrient solutions as a normal homogeneous clear solution. We also assume that Zn<sup>2+</sup>, PO<sub>4</sub><sup>3-</sup> and DABCO ions act as a source of inactive species and there is formation of certain other ‘active’ species by combining these ions and that are contributing to crystal growth. The values of constants and parameters used in the simulation are given in Table 1. The change in concentration of both inactive,  $I$ , and active,  $C$ , species are shown in Figure 7a. It is observed that the concentration of inactive species decreases exponentially as expected according to Equation 10. The concentration of active species,  $C$ , increases to some level above the final value of 0.04 mole/cm<sup>3</sup> and then decreases to this level as growth consumes the intermediate.

Table 1. Values of constants and parameters used in simulations.

Symbol	Value
$I_0$	0.05 mole/cm <sup>3</sup>
$C_{critical}$	0.04 mole/cm <sup>3</sup>
$k_g$	5.4 $\mu\text{m cm}^3 / \text{min mole}$
$\phi$	6.0
$\rho$	$1.0 \times 10^{-14}$ mole/ $\mu\text{m}^3$
$k_1$	0.18 min <sup>-1</sup>
$n_0$	$1.0 \times 10^{10}$
$r$	$7.5 \times 10^{-3}$ $\mu\text{m}$

The average particle sizes determined by light scattering are plotted in Figure 7b along with the experimental data, which shows that the simulation of average crystal size reaches to a final value. There is a time lag before crystals begin to grow. This time lag stems from the fact that the concentration of intermediate, C, must build up to a certain level,  $C_{critical}$ , before it can start attaching to the crystals to begin crystal growth.

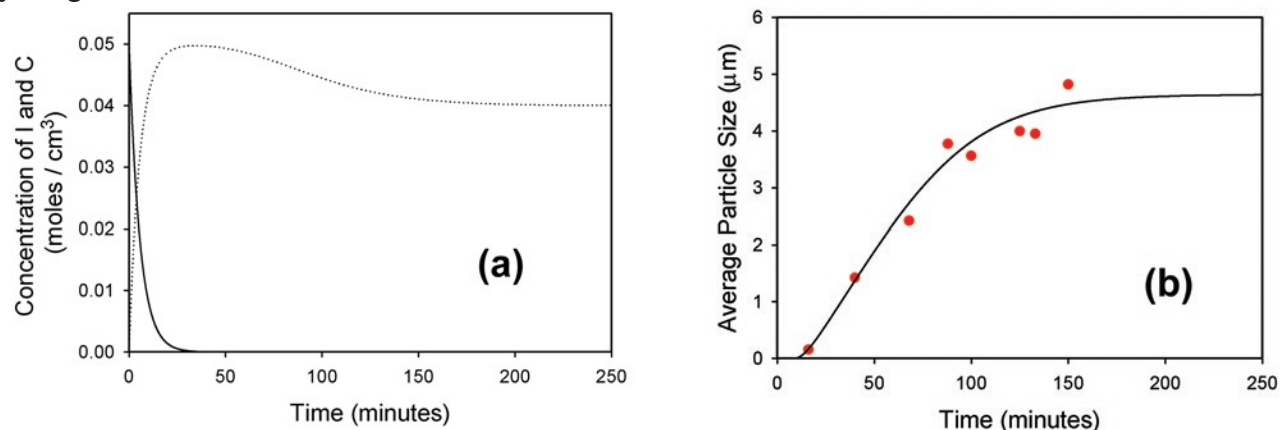


Figure 7. (a) Plot of variation of concentration of active and inactive species vs. time and (b) fitting of the calculated average particle size with the experimental data.

## 5. Proposed Experiments in Microgravity

Two major effects are manifested in microgravity. Under gravitational conditions, particles with densities greater than the fluid will settle with a terminal velocity as defined by Stokes law. Under microgravity conditions, the settling rate can be slowed down by 4 to 6 orders of magnitude. For example, in gravity of  $10^{-4}g$ , a 10-micron ZnPO particles will sediment about one cm in about 3 days. The second effect of microgravity is to reduce buoyancy driven convection. The convection process can be visualized as follows. The growth of the crystal leads to depletion of nutrients around it. This depleted volume will rise because it is lighter, leading to convection. This can limit the contact between the growing particle and nutrient as well as bring fresh nutrient towards the particle, thereby influencing crystal growth dynamics. Approximate calculations assuming a density differential of 0.01 g/cc lead to fluid flows of  $10^{-4}cm/sec$  at 1g, as compared to  $10^{-6}cm/sec$  at  $10^{-4}g$  around a 1 micron crystal of zincophosphate sodalite. Our goal is to exploit this effect to deduce information about crystal growth/dissolution.

### 5.1 Detachment Process

The goal here is to examine the difference in dissolution of two zincophosphate structures, sodalite and faujasite. There appears to be some consensus that growth of microporous structures occur by attachment of pseudocell units. *But, how do frameworks dissolve? Is it "atom-by-atom" or do polyhedral segments characteristic of the framework dissociates from the crystal.* If identical experiments are repeated on ground and microgravity, then from the measured velocity, the diffusion coefficient  $D_i$  can be unambiguously determined. Comparison of  $D_i$  between sodalite and faujasite structure fragments should readily indicate differences in size of the dissolving unit. Similar  $D_i$ 's will suggest dissolution by a pathway approaching an atom-by-atom dissolution.

## 5.2 Crystal Growth Experiments

The second set of experiments we propose to do in microgravity involves the growth of ZnPO-X and ZnPO-S from reactants in reverse micelles. Both these structures have sodalite units as building blocks, with the difference in microporosity arising from the packing of these units. We will examine the crystal growth dynamics for identical reactant compositions under microgravity and earth-based conditions using laser light scattering. *The hypothesis we want to verify is that the molecular complexity of the attaching species on a growing crystal surface changes with the framework.* At this stage, we are not proposing to discover the molecular structures of these species, but rather their complexity, e.g. are these atomic or polyhedral units? Typically, these pseudocell units have a convective-diffusive flow around the growing crystal. *Convection-driven shearing force will influence the rates of crystal growth differently for different frameworks.* The more complex the attaching species, the greater will be the influence of convection. The advantage of using the reverse micellar system is that a layer-by-layer crystal growth process is possible and the growth can be followed by light scattering. *Microgravity provides an environment in which the chemistry remains the same, yet the lack of convection can change the crystal growth dynamics for the same framework.* How this change is manifested differently for sodalite and faujasite is the information we are after.

## Acknowledgement

We acknowledge funding from NASA for this research.

## References

1. Singh, R., Doolittle, Jr. J., and Dutta, P.K. Aqueous transformations of zincophosphate microporous materials: influence of framework topology. *J. Phys. Chem. B*, vol. 106, 2146-2152 (2002).
2. Castagnola, M.J., and Dutta, P.K. Raman microprobe studies of dissolution of microporous faujasitic-like zincophosphate crystals. *Microporous and Mesoporous Materials*, vol. 42, 235-243 (2001).
3. Singh, R., Castagnola, M.J., and Dutta, P.K. in "Reactions and Synthesis in Surfactant Systems", Texter, J. (Editor), Marcel-Dekker, New York, vol. 100, 737-760 (2001).
4. Singh, R., and Dutta, P.K. Crystal growth of fujasitic microporous zincophosphate crystals using reverse micelles as reactants. *Langmuir*, vol. 16, 4148-4153 (2000).
5. Castagnola, M.J., and Dutta, P.K. Synthesis of microporous faujasitic-like zincophosphates from reverse micelles. *Microporous and Mesoporous Materials*, vol. 34, 61-65 (2000).
6. Castagnola, M. J., and Dutta, P.K. Crystal growth of zincophosphates from conventional media and reverse micelles: mechanistic implications. *Microporous Mesoporous Mater.*, vol. 20, 149-159 (1998).
7. Reddy, K.S.N., Salvati, L.M., Dutta, P.K., Abel, P.B., Suh, K.I., and Ansari, R.R. Reverse Micelle Based Growth of Zincophosphate Sodalite: Examination of Crystal Growth. *J. Phys. Chem.*, vol. 100, 9870-9880 (1996).
8. Dutta, P.K., Jakupca, M., Reddy, K.S.N., and Salvati, L. Controlled growth of microporous crystals nucleated in reverse micelles. *Nature (London)*, vol. 374, 44-46 (1995).
9. Castagnola, M.J., and Dutta, P.K. "Synthesis of Platelet-Like Faujasitic Zincophosphate X Crystals." *Proceedings of the 12<sup>th</sup> International Zeolite Conference*, Materials Research Society, 1627-1632 (1999).
10. Pillai, V., Kumar, P., Hou, M. J., Ayyub, P., and Shah, D. O. Preparation of nanoparticles of silver halides, superconductors and magnetic materials using water-in-oil microemulsions as nano-reactors. *Adv. Colloid Interface Sci.* vol. 55, 241-69 (1995).

11. Gonthier, S., and Thompson, R. W. Effects of seeding on zeolite crystallization, and the growth behavior of seeds. *Stud. Surf. Sci. Catal. Vol. 85*(“Advanced Zeolite Science and Applications”), 43-73. (1994).
12. Schoeman, B. J., Sterte, J., and Otterstedt, J.-E. Colloidal zeolite suspensions. *Zeolites* vol. 14, 110-116 (1994).
13. Schoeman, B. J., Sterte, J., and Otterstedt, J.-E. The synthesis of colloidal zeolite hydroxysodalite sols by homogeneous nucleation. *Zeolites* vol. 14, 208-216 (1994).
14. Anderson, M. W., Agger, J. R., Thornton, J. T., Forsyth, N. Crystal growth in zeolite Y revealed by atomic force microscopy. *Angew. Chem., Int. Ed. Engl. Vol. 35*, 1210-1213. (1996).
15. Thompson, R. W. Population balance analysis of zeolite crystallization. “Modelling of Structure and Reactivity in Zeolites” (Catlow, C. R. A., Editor), Academic Press, New York, 231-255 (1992).
16. Ouden, C. J. J. D., and Thompson, R. W. Analysis of the formation of monodisperse populations by homogeneous nucleation. *J. Coll. Inter. Sci.* vol. 143, 77-84 (1991).
17. Bandyopadhyaya, R., Kumar, R., and Gandhi, K. S. Modelling of CaCO<sub>3</sub> nanoparticle formation during overbasing of lubricating oil additives. *Langmuir* vol. 17, 1015-1029 (2001).
18. Sato, H., Asaji, N., and Komasaawa, I. A population balance approach for particle coagulation in reverse micelles. *Ind. Eng. Chem. Res.* vol. 39, 328-334 (2000).
19. Matsoukas, T., and Gulari, E. Monomer-addition growth with a slow initiation step: a growth model for silica particles from alkoxides. *J. Coll. Inter. Sci.* vol. 132, 13-21 (1989).